Electrical detection of ferroelectriclike metals through the nonlinear Hall effect

Rui-Chun Xiao

Ding-Fu Shao

Wenjuan Huang

Hua Jiang

Electrical detection of ferroelectriclike metals through the nonlinear Hall effect

Rui-Chun Xiao [1,2] Ding-Fu Shao [3,*] Wenjuan Huang,[4] and Hua Jiang[1,2,†]

[1]*School of Physical Science and Technology, Soochow University, Suzhou 215006, China*
[2]*Institute for Advanced Study, Soochow University, Suzhou 215006, China*
[3]*Department of Physics and Astronomy & Nebraska Center for Materials and Nanoscience, University of Nebraska, Lincoln, Nebraska 68588-0299, USA*
[4]*Changzhou Institute of Technology, Changzhou 213031, China*

Ferroelectriclike metals are a relatively rare class of materials that have ferroelectriclike distortion and metallic conductivity. $LiOsO_3$ is the first demonstrated and the most investigated ferroelectriclike metal. The presence of free carriers makes them difficult to be studied by traditional ferroelectric techniques. In this paper, using symmetry analysis and first-principles calculations, we demonstrate that the ferroelectriclike transition of $LiOsO_3$ can be probed by a kind of electrical transport method based on nonlinear Hall effect. The Berry curvature dipole exists in the ferroelectriclike phase and it can lead to a measurable nonlinear Hall conductance with a conventional experimental setup. However, the symmetry of the paraelectriclike phase $LiOsO_3$ vanishes the Berry curvature dipole. The Berry curvature dipole shows a strong dependence on the polar displacement, which might be helpful for the detection of polar order. The nonlinear Hall effect provides an effective method for the detection of phase transition in the study of the ferroelectriclike metals and promotes them to be applied in ferroelectriclike electronic devices.

I. INTRODUCTION

Ferroelectrics are a kind of crystalline material that exhibit electrically switchable electrical polarization. In these types of materials, the structural phase transitions happen at the ferroelectric critical temperature, bringing the spontaneous atomic polar distortion and ferroelectric polarization at low temperatures. The ferroelectric materials are usually insulators. In the 1960s, Anderson and Blount pointed out that in a metallic system, a ferroelectric-like structural phase transition can also emerge to introduce the long-range polar order [1]. Due to the coexistence of two seemingly incompatible properties: ferroelectriclike distortion and metallic conductivity, the ferroelectriclike metals are a relatively rare class of materials. This concept was first found in $LiOsO_3$ [2], and then was found in $NdNiO_3$ thin film [3] and some Van der Waals materials such as WTe_2 [4,5] and $MoTe_2$ [6], etc. The combination of metallicity and polar structures gives rise to a series of unique physical properties, such as unconventional Cooper pairing [7–10], highly anisotropic thermopower response [10], anomalous optical properties [11,12], and magnetoelectricity [7,10,13].

Despite these remarkable signs of progress, the efficient detection of the polar order in ferroelectriclike metal remains a challenging problem. The screen of the conduction electron makes it difficult to be characterized by traditional techniques such as piezo-force microscopy and ferroelectric hysteresis loop measurements. Structural characterization methods such as x-ray and neutron diffraction can be used to detect the ferroelectriclike phase transition [2]. However, it is difficult to distinguish whether the polar displacement is positive or negative in these methods. Optical techniques such as nonlinear optical method (second harmonic generation) [3,14,15] can probe the structural asymmetry in ferroelectriclike metals. However, the strong absorption of light by metals limits the detection within small thicknesses below the surface. Thus, an efficient electrical transport method to detect the ferroelectriclike transition and polar order would be desirable for ferroelectriclike metals.

This difficulty might be solved by the recently discovered nonlinear Hall effect [16,17]. Unlike the linear anomalous Hall effect that only appears in magnetic materials where the time-reversal symmetry $\hat{T}$ is broken, the nonlinear Hall effect can emerge in nonmagnetic (i.e., $\hat{T}$ is invariant) materials as a second-order response to an electric field. It requires the breaking of inversion symmetry $\hat{I}$ and finite Berry curvature dipole to generate a net anomalous velocity in a metallic system under the application of charge current. This effect has been experimentally observed in few-layer WTe_2 [18,19] and monolayer strained MoS_2 [20]. It was demonstrated that the Berry curvature dipole could be used to detect the ferroelectric order in two-dimensional ferroelectric materials, such as few-layer WTe_2 [21,22] and $SnTe$ [23,24]. Since all ferroelectriclike metals have a noncentrosymmetric polar structure, the nonlinear Hall effect is an intrinsic property of these materials. Therefore, the nonlinear Hall effect can be used to detect the polar order in them.

In this paper, we use the most investigated ferroelectriclike metal $LiOsO_3$ as a representative material to demonstrate that the polar order in ferroelectriclike metals can be detected by

*dfshao@unl.edu
†jianghuaphy@suda.edu.cn

the nonlinear Hall effect. Based on the symmetry analysis and first-principles density-functional theory (DFT) calculations, we predict that the paraelectriclike phase of LiOsO$_3$ prohibits the existence of the nonlinear Hall effect, while the ferroelectriclike LiOsO$_3$ supports a sizable Berry curvature dipole and leads to a measurable nonlinear Hall voltage.

The rest of the paper is arranged as follows. In Sec. II, the symmetry analysis of the nonlinear Hall effect is performed. In Sec. III, we introduce the first-principles calculation methods. The calculation results and the corresponding explanation of the calculation results are shown in Sec. IV. Discussion is listed in Sec. V, and a brief conclusion is given in Sec. VI.

II. SYMMETRY ANALYSIS

An electric field $\mathbf{E} = \mathrm{Re}\{Ee^{i\omega t}\}$ with amplitude E and frequency ω can introduce the nonlinear Hall current density [16],

$$J_a = \mathrm{Re}\{J_a^{(0)} + J_a^{(2)}e^{i2\omega t}\}, \qquad (1)$$

where $a, b, c = \{x, y, z\}$, $J_a^{(0)} = \chi_{abc}^{(0)}E_bE_c^*$ describes the rectified current and $J_a^{(2)} = \chi_{abc}^{(2)}E_bE_c$ is the second harmonic current. Here the nonlinear Hall coefficients are

$$\chi_{abc}^{(0)} = \chi_{abc}^{(2)} = -\epsilon_{adc}\frac{e^3\tau D_{bd}}{2\hbar^2(1+i\omega\tau)}, \qquad (2)$$

which include the relaxation time τ and the Berry curvature dipole D_{bd}:

$$D_{bd} = \int\frac{d^3\mathbf{k}}{(2\pi)^3}\rho_{bd}(\mathbf{k}) = -\int\frac{d^3\mathbf{k}}{(2\pi)^3}\sum_n v_b\Omega_{n\mathbf{k}}^d\frac{\partial f_0}{\partial E_{n\mathbf{k}}}. \qquad (3)$$

Here ρ_{bd} is the Berry curvature dipole density, $E_{n\mathbf{k}}$ is the energy of the nth band at the $\mathbf{k}$ point, f_0 means the equilibrium Fermi-Dirac distribution function, and $\Omega_{n\mathbf{k}}^d$ denotes the Berry curvature. Finite D_{bd} can emerge in a nonmagnetic (i.e., $\hat{T}$ is invariant) material within inversion symmetry $\hat{I}$ broken [16]. Clearly, the factor $\partial f_0/\partial E_{n\mathbf{k}}$ in Eq. (3) indicates that the Berry curvature dipole is a Fermi surface property and the nonlinear Hall effect can only appear in metallic systems.

All the polar point groups (C_n, C_{nv} $n = 1, 2, 3, 4, 6$) can have nonzero Berry curvature dipole. In these polar groups, it is convenient to define a vector $\mathbf{d}$ [16] as $d_a = \epsilon_{abc}D_{bc}^-/2$, where $D^- = (D - D^T)/2$ is the antisymmetric parts of the Berry curvature dipole tensor. The polar symmetry enforces the finite vector $\mathbf{d}$ oriented along the polar axis [16], which is something similar to the electric dipole $\mathbf{P}$ in ferroelectric insulators. Ferroelectriclike metals are metallic systems with noncentrosymmetric polar structures. Therefore, the polar phase can be directly reflected by the nonlinear Hall response related to the vector $\mathbf{d}$. Above the critical temperature, these materials transform from the ferroelectriclike phase to the paraelectriclike phase. The paraelectriclike phase has zero Berry curvature dipole due to the existence of inversion symmetry. This phase transition can change the magnitude of the nonlinear Hall voltage from a finite value to zero. If the polar displacement is switched, the nonlinear Hall voltage will be reversed, because this switching is equivalent to an inversion symmetry operation, which changes the sign of the Berry curvature dipole. This fully shows that the nonlinear Hall effect
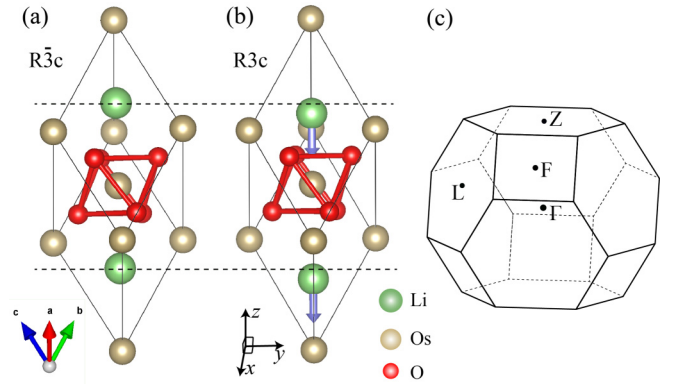

FIG. 1. Primitive unit cell of (a) paraelectriclike and (b) ferroelectriclike phases of LiOsO$_3$. The ferroelectriclike phase transition mainly involves the displacements of Li atoms. The arrows in (b) stand for the displacements of Li ions along the polar axis (z direction). (c) Brillouin zone of LiOsO$_3$.

measurement can be a promising method for the electrical detection of the polar order in the ferroelectric-like metals.

Here we use LiOsO$_3$, the first discovered [2] and most investigated [14,25–28] ferroelectric-like metal, as a representative example to demonstrate that the nonlinear Hall effect can detect the polar order in ferroelectriclike metals. At high temperature, LiOsO$_3$ has a centrosymmetric rhombohedral structure with space group $R\bar{3}c$ (No. 167) and point group D_{3d}. The Os atom is octahedrally coordinated by six O atoms and located at the center between two Li atoms [Fig. 1(a)]. In this paraelectriclike phase, the Berry curvature dipole vanishes due to the inversion symmetry $\hat{I}$. A ferroelectriclike structural transition shows up below 140 K [2] due to the A_{2u} phonon module of the paraelectriclike phase [25,26], accompanied by the main displacement of Li atoms along the polar direction, i.e., z ([111]) direction. This displacement results in a ferroelectriclike phase with space group $R3c$ (No. 161) and point group C_{3v}, as shown in Fig. 1(b). This point group contains a threefold rotation symmetry C_{3z} around z direction, and three mirror planes parallel to the z direction. The Berry curvature dipole tensor under point group C_{3v} is (see Supplemental Material [29]):

$$D = \begin{bmatrix} 0 & D_{xy} & 0 \\ -D_{xy} & 0 & 0 \\ 0 & 0 & 0 \end{bmatrix}. \qquad (4)$$

There are only two independent nonzero antisymmetric elements. This leads to the vector $\mathbf{d} = (0, 0, d_z)$ oriented along the polar axis with $d_z = (D_{xy} - D_{yx})/2 = D_{xy}$, which relates to a nonlinear Hall current along z direction induced by an in-plane injecting current (see details in Sec. IV).

III. CALCULATION DETAILS

The first-principles calculations based on DFT are performed with the projector augmented-wave method implemented in the VASP [30,31] package. General gradient approximation based on the Perdew-Burke-Ernzerhof (functional is used and the spin-orbit coupling effect is included. The Brillouin zone is sampled with a $16 \times 16 \times 16$ mesh of k points.

TABLE I. Calculated lattice parameters and the polar displacement of the Li atom with the hexagonal representation. The numbers inside the parentheses are the experimental values reported in Ref. [2].

	a (Å)	c (Å)	Δz_{Li} (Å)	ΔE (meV)
Paraelectriclike LiOsO$_3$	5.164 (5.064)	13.178 (13.211)	0	0
Ferroelectriclike LiOsO$_3$	5.091 (5.046)	13.362 (13.239)	0.479 (0.467)	−56

The lattice parameters and atomic positions are fully relaxed until the force on each atom is less than 10^{-4} eV/Å. The DFT Bloch wave functions are iteratively transformed into maximally localized Wannier functions by the WANNIER90 code [32,33] and Os-d and O-p orbitals are used to construct the Wannier functions. The Berry curvature and Berry curvature dipole are calculated by the Wannier function implemented in the WANNIERTOOLS software package [34]. In the Berry curvature dipole calculations, the adaptive broadening scheme for k-space integration [35] is employed. The convergence test is taken, and a k-mesh grid of $300 \times 300 \times 300$ is adopted.

IV. RESULTS AND EXPLANATIONS

The calculated crystal structural parameters and total energies of the LiOsO$_3$ are shown in Table I. We find the calculated lattice constants and atomic displacement are close to the experimental and previously calculated values [2,25,27]. The ferroelectriclike phase of LiOsO$_3$ has lower energy by 56 meV/cell compared to the paraelectriclike phase. This result is consistent with the experimental observations that the ferroelectriclike phase is the ground state at low temperature [2].

The calculated band structures of the paraelectriclike and ferroelectriclike LiOsO$_3$ are shown in Figs. 2(a) and 2(b), respectively. Consistent with previous theoretical works [25,27,36], we find the bands around the Fermi energy (E_F) are mainly contributed by the Os-d and O-p orbitals (see Fig. S1 in the Supplemental Material [29]). Since Li atoms are highly ionic and do not bond with Os and O atoms, the polar displacements of Li do not influence the major shape of the band structures around E_F. The main difference between the band structures of the two phases is degeneracy. In the paraelectriclike phase, the presence of the inversion symmetry $\hat{I}$ and time-reversal symmetry $\hat{T}$ enforces the double degeneracy of each band in the Brillouin zone. On the other hand, the inversion symmetry $\hat{I}$ is removed in the ferroelectriclike phase, which destroys the band degeneracy except for the
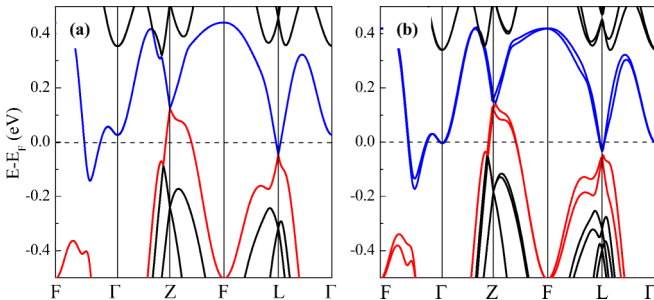
time-reversal invariant **k** points. Here we focus on the band structure of the ferroelectriclike phase. There are four bands crossing the E_F, forming holelike pockets at the top and bottom surfaces of the Brillouin zone and electronlike pockets around the center and the corners of Brillouin zone, as shown in Fig. S1 [29]. Figure 3(a) shows the cross section of the Fermi pockets when $k_z = 0$, where the threefold rotation $\hat{C}_{3z}$ and three mirror $\hat{m}$ symmetries are clearly reflected.

As described by the symmetry analysis in Sec. II, the metallic ground state and the polar structure guarantee the existence of the Berry curvature dipole in ferroelectriclike LiOsO$_3$. This can be seen from the transformations of Berry curvature dipole density ρ_{bd} under symmetry operations reflected by our numerical calculations. For example, the mirror symmetry $\hat{m}_{xz}$ generates the symmetry transformations of the **k** point, velocity, and Berry curvature: $\hat{m}_{xz}(k_x, k_y, k_z) = (k_x, -k_y, k_z)$, $\hat{m}_{xz}v_x(k_x, k_y, k_z) = v_x(k_x, -k_y, k_z)$, and $\hat{m}_{xz}\Omega_n^y(k_x, k_y, k_z) = \Omega_n^y(k_x, -k_y, k_z)$, as shown in Fig. 3(a). Therefore, $\rho_{xy} = -\sum_n v_x \Omega_{n\mathbf{k}}^y \frac{\partial f_0}{\partial E_{n\mathbf{k}}}$ is symmetric with $\hat{m}_{xz}$ operation, i.e., $\hat{m}_{xz}\rho_{xy}(k_x, k_y, k_z) = \rho_{xy}(k_x, -k_y, k_z)$, as shown in Fig. 3(b). As a result, the Berry curvature dipole component $D_{xy} = \int \frac{d^3\mathbf{k}}{(2\pi)^3} \rho_{xy}$ is nonzero. For another, the $\rho_{xx} = -\sum_n v_x \Omega_{n\mathbf{k}}^x \frac{\partial f_0}{\partial E_{n\mathbf{k}}}$ is asymmetrically distributed with respect to the mirror plane $\hat{m}_{xz}$ [Fig. 3(c)]
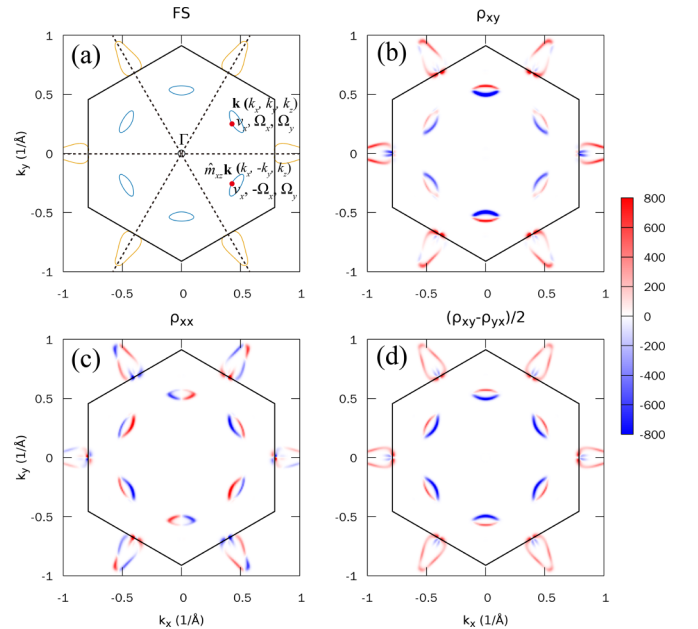

FIG. 3. (a) Fermi surface of ferroelectriclike LiOsO$_3$. Berry curvature dipole density (in Å^3) of (b) $\rho_{xy}(\mathbf{k})$, (c) $\rho_{xx}(\mathbf{k})$, and (d) $[\rho_{xy}(\mathbf{k}) - \rho_{yx}(\mathbf{k})]/2$ of ferroelectriclike LiOsO$_3$ for $k_z = 0$ plane. The dashed lines in (a) denote the mirror planes and the hexagons mean the Brillouin zone boundary.

FIG. 2. Band structure of (a) paraelectriclike and (b) ferroelectriclike LiOsO$_3$.
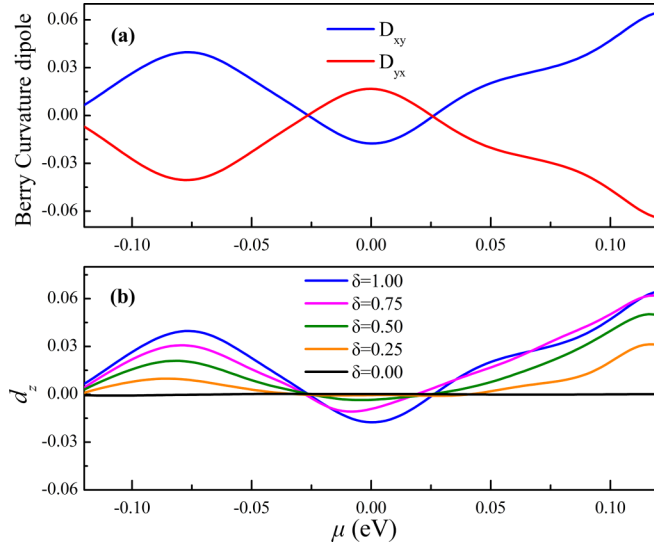
FIG. 4. (a) D_{xy} and D_{yx} as a function of the chemical potential μ for the ferroelectriclike LiOsO$_3$. (b) The evolution d_z with polar order.

due to $\hat{m}_{xz}\Omega_n^x(k_x, k_y, k_z) = -\Omega_n^x(k_x, -k_y, k_z)$, which leads to $\hat{m}_{xz}\rho_{xx}(k_x, k_y, k_z) = -\rho_{xx}(k_x, -k_y, k_z)$. Therefore, $D_{xx} = \int \frac{d^3\mathbf{k}}{(2\pi)^3}\rho_{xx} = 0$. The whole symmetries of velocity and Berry curvature under C_{3v} symmetry are shown in Table S1 in the Supplemental Material [29]. Similarly, we can check the symmetry distribution of other ρ_{bd}. The combination of the antisymmetric parts of Berry curvature dipole density $[\rho_{xy}(\mathbf{k}) - \rho_{yx}(\mathbf{k})]/2$ has threefold symmetry and distributes symmetrically with respect to the three mirror planes, as shown in Fig. 3(d), due to $\rho_{xy}(\mathbf{k}) - \rho_{yx}(\mathbf{k}) = \rho_{xy}(\hat{C}_{3z}^+\mathbf{k}) - \rho_{yx}(\hat{C}_{3z}^+\mathbf{k}) = \rho_{xy}(\hat{C}_{3z}^-\mathbf{k}) - \rho_{yx}(\hat{C}_{3z}^-\mathbf{k})$ (see Supplemental Material [29]). These results indicate that our numerical calculations are consistent with the symmetry. Besides, only the $\mathbf{k}$ points located at the Fermi surface have nonzero ρ_{bd} as shown in Fig. 3, which implies Berry curvature dipole is indeed the property of Fermi surface.

Figure 4(a) shows the calculated Berry curvature dipole as a function of the chemical potential. $D_{xy} = -D_{yz}$, which is consistent with the above symmetry analysis. The calculated Berry curvature dipole is about 0.017 at E_F and can be enhanced by proper doping. The Berry curvature dipole is comparable to those predicted in Weyl semimetals TaAs, MoTe$_2$ [37], and topological insulator BiTeI [38]. There are some band crossings near E_F in ferroelectriclike LiOsO$_3$ [36]. However, we note they do not have notable contributions to the Berry curvature dipole due to the small tilting [29]. Similar situations have been found in some topological semimetals recently [37,39]. We found the Hubbard U will change the band structures and Berry curvature dipole accordingly (see Supplemental Material [29]). However, the nonlinear Hall effect still exists in the ferroelectriclike LiOsO$_3$, because it is determined by the symmetry.

To show the dependence of D_{xy} on the polar order, we manually move the atoms along the z direction and define δ as a parameter to reflect the polar displacement. $\delta = 0$ corresponds to the paraelectriclike LiOsO$_3$ phase, while $\delta =$

1 corresponds to the ferroelectriclike phase. As shown in Fig. 4(b), the magnitude of d_z monotonically decreases with δ and vanishes in the paraelectriclike phase ($\delta = 0$). Clearly, the ferroelectriclike phase transition can be reflected by the change of the nonlinear Hall voltage.

Next, we discuss the nonlinear Hall response induced by the Berry curvature dipole in ferroelectriclike LiOsO$_3$. In the polar group system with Berry curvature dipole $\mathbf{d}$, the nonlinear Hall current density driven by an electrical field $\mathbf{E}$ can be written as [16]

$$
\begin{cases}
\mathbf{J}^0 = \frac{e^3\tau}{2\hbar^2(1+i\omega\tau)}\mathbf{E}^* \times (\mathbf{d} \times \mathbf{E}) \\
\mathbf{J}^{2\omega} = \frac{e^3\tau}{2\hbar^2(1+i\omega\tau)}\mathbf{E} \times (\mathbf{d} \times \mathbf{E}).
\end{cases}
\tag{5}
$$

For an electric field $\mathbf{E} = Ee^{i\omega t}(\sin\theta\cos\varphi, \sin\theta\sin\varphi, \cos\theta)$ (θ is the polar angle relative to the z axis, and φ is the azimuthal angle relative to the x axis), the induced nonlinear Hall current density,

$$
|\mathbf{J}^0| = |\mathbf{J}^{2\omega}| = \frac{e^3\tau d_z E^2}{2\hbar^2(1+i\omega\tau)}
$$

$$
\times [-\cos\theta\sin\theta\cos\varphi, -\cos\theta\sin\theta\sin\varphi, \sin^2\theta]. \tag{6}
$$

Clearly, the nonlinear Hall current is absent when the electric field $\mathbf{E}$ is along the z axis ($\theta = 0°$), according to Eq. (6). When the electric field $\mathbf{E}$ is parallel to the $x - y$ plane ($\theta = 90°$), the in-plane component of the nonlinear Hall current vanishes, while the out-of-plane component exists. Moreover, according to Eq. (6), it is independent with the azimuthal angle φ. This angle dependence of the nonlinear Hall effect in LiOsO$_3$ is much simpler than that of the nonlinear optics experiment [15], indicating the convenience to detect the polar order. Besides, different from the nonlinear optical method used in ferroelectriclike metal [3,15], the nonlinear Hall current flows inside the bulk of metals, which means the influence of the surface is small.

In the DC limit ($\omega \rightarrow 0$), the nonlinear Hall conductance induced by an in-plane electric field is

$$
\sigma^{\text{NHE}} = (J^{(0)} + J^{(2\omega)})/E = \frac{e^3\tau d_z E}{\hbar^2}. \tag{7}
$$

In the constant relaxation-time approximation, the Ohmic conductivity is expressed as [35]

$$
\sigma_{ab} = \frac{e^2\tau}{\hbar^2}C_{ab}, \tag{8}
$$

where

$$
C_{ab} = \int \frac{1}{(2\pi)^3}\sum_n \frac{\partial E_{n\mathbf{k}}}{\partial k_a}\frac{\partial E_{n\mathbf{k}}}{\partial k_b}\left(-\frac{\partial f_0}{\partial E_{n\mathbf{k}}}\right). \tag{9}
$$

The parameter C can be easily obtained in our DFT calculations (see Fig. S3 in the Supplemental Material [29]). Using Eqs. (8) and (9), we can drop out of the relaxation-time τ in Eq. (7). Therefore, the nonlinear Hall conductivity in the DC limit can be simply estimated by

$$
\sigma^{\text{NHE}} = e\frac{d_z}{C_\perp}J. \tag{10}
$$

Using the calculated $d_z \sim 0.02$ and $C_\perp \sim 0.02$ eV/Å ($\perp$ means the $x - y$ direction, e.g., C_{xx}) in the ferroelectriclike
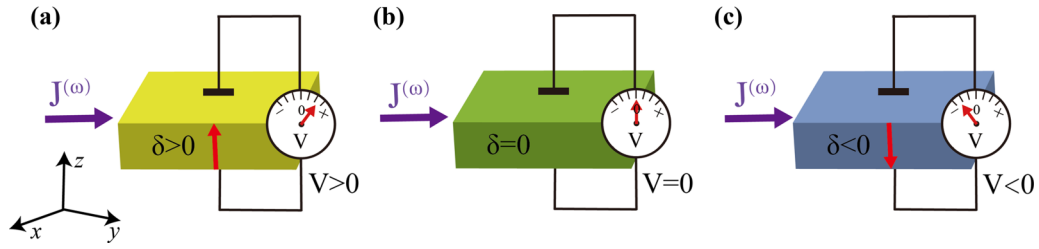
FIG. 5. (a) Schematics of the polar order detection in ferroelectriclike metal by the nonlinear Hall effect. The paraelectriclike and ferroelectriclike state of $LiOsO_3$ are all metallic; therefore, the driving current can go through the $x - y$ plane (perpendicular to the polar axis). An in-plane charge current generates a nonlinear Hall voltage along the out-of-plane direction, which is determined by the polar displacement (denoted by δ). The nonlinear Hall voltage is (a) positive for $\delta > 0$, (b) zero for $\delta = 0$, and (c) negative for $\delta < 0$.

$LiOsO_3$ and a conventional driving electric current $J \sim 5 \times 10^6$ A/cm^2, the calculated nonlinear Hall conductance of $\sigma^{NHE} \sim 5$ Ω^{-1}m^{-1} is estimated, according to Eq. (10). The sizable nonlinear Hall conductance is comparable to those values of anomalous Hall materials [40]. Furthermore, as shown in Eq. (1), the nonlinear Hall current introduced by a high-frequency electric field can be decomposed into a rectified current and a second harmonic one. It allows us to easily distinguish the output signal from the input current by frequency. To sum up, the nonlinear Hall effect measurement is really a promising and efficient detection method for the polar order in $LiOsO_3$.

V. DISCUSSION

The manipulation and detection of the magnetic or electric dipoles result in spintronic and ferroelectric electronic devices. Similarly, the manipulation and detection of the polar order in ferroelectriclike metals might also generate promising electronic devices. However, the screen effect from the conduction electrons seems to prohibit the electrical switching and detection of the polar order in ferroelectriclike metals, which limits the electronic applications of these materials. It was suggested that the pressure and strain could be used to control the polar displacement of ferroelectric metals such as $LiOsO_3$ [41,42]. Theoretical proposals have been made for the electrical reversal of the polar distortion in ferroelectriclike metals, such as decreasing the ferroelectriclike metal thickness [28], using the interface coupling between the ferroelectriclike metal and the ferroelectric insulating substrate [26,43], etc. Experimentally, the switching of the ferroelectriclike metal has been demonstrated in few-layer WTe_2 by using a double gate device [4] and in bulk WTe_2 single crystals using a piezoresponse force microscopy [5]. Despite this remarkable progress, the efficient detection of the polar order in ferroelectriclike metals remains a challenging problem.

Our calculation shows that the nonlinear Hall effect can reflect not only the ferroelectriclike phase transition but also the polar order of $LiOsO_3$. If d_z is positive for the positive polar displacement ($\delta > 0$), a positive Hall voltage appears along the z direction, as shown in Fig. 5(a). On the other hand, the switching of the polar direction is equivalent to apply the inversion symmetry operation in $LiOsO_3$, which

changes the sign of the Berry curvature dipole and thus reverses the nonlinear Hall voltage [Fig. 5(c)]. However, the paraelectriclike state cannot generate the nonlinear Hall signal due to the symmetry [Fig. 5(b)]. This strong dependence of the nonlinear Hall voltage on the polar direction is expected to be robust against the unavoidable doping effect by defects, because the sign of d_z remains invariable in a broad energy window of 40 meV around E_F (Fig. 4). In addition to $LiOsO_3$, other ferroelectriclike metals such as $Ca_3Ru_2O_7$ [44], $Cd_2Re_2O_3$ [45,46], GeTe [47], $NdNiO_3$ [3], etc. [48–50] are also promising candidates to host nonlinear Hall effects. The manipulation and detection of polar order in ferroelectriclike metals will be beneficial to expand the corresponding electronic applications.

Due to the limitation of DFT calculations, we only consider the intrinsic contribution of the nonlinear Hall effect in this paper. Disorder and impurity scattering can also have extrinsic contributions to the nonlinear Hall effect, as claimed in recent theoretical works [51–55]. Both the intrinsic and extrinsic nonlinear Hall effect require a noncentrosymmetric crystal space group. Therefore, ferroelectriclike metals guarantee the existence of the nonlinear Hall effect. Moreover, the intrinsic and extrinsic nonlinear Hall signals may have different frequency dependence on the applied electric field [52] and temperature [55], which offers the methods to figure out the major contribution of nonlinear Hall effect.

VI. CONCLUSION

In conclusion, we propose that the nonlinear Hall effect can detect polar order in ferroelectriclike metals. As a representative example, we consider the most investigated ferroelectriclike metal $LiOsO_3$ and show that it has a large Berry curvature dipole, which can introduce a sizable nonlinear Hall effect. This effect disappears in the paraelectriclike phase. Moreover, the strong dependence of the Berry curvature dipole on the polar displacement offers an efficient method to detect the polar order. Therefore, the nonlinear Hall effect can be used in the study of the ferroelectriclike structural phase transition and expands potential applications in ferroelectriclike electronic devices. We hope our prediction will stimulate the experimental exploration of the nonlinear Hall effect in ferroelectriclike metals.

[1] P. W. Anderson and E. I. Blount, Phys. Rev. Lett. **14**, 217 (1965).

[2] Y. Shi, Y. Guo, X. Wang, A. J. Princep, D. Khalyavin, P. Manuel, Y. Michiue, A. Sato, K. Tsuda, S. Yu, M. Arai, Y. Shirako, M. Akaogi, N. Wang, K. Yamaura, and A. T. Boothroyd, Nat. Mater. **12**, 1024 (2013).

[3] T. H. Kim, D. Puggioni, Y. Yuan, L. Xie, H. Zhou, N. Campbell, P. J. Ryan, Y. Choi, J. W. Kim, J. R. Patzner, S. Ryu, J. P. Podkaminer, J. Irwin, Y. Ma, C. J. Fennie, M. S. Rzchowski, X. Q. Pan, V. Gopalan, J. M. Rondinelli, and C. B. Eom, Nature **533**, 68 (2016).

[4] Z. Fei, W. Zhao, T. A. Palomaki, B. Sun, M. K. Miller, Z. Zhao, J. Yan, X. Xu, and D. H. Cobden, Nature **560**, 336 (2018).

[5] P. Sharma, F.-X. Xiang, D.-F. Shao, D. Zhang, E. Y. Tsymbal, A. R. Hamilton, and J. Seidel, Sci. Adv. **5**, eaax5080 (2019).

[6] S. Yuan, X. Luo, H. L. Chan, C. Xiao, Y. Dai, M. Xie, and J. Hao, Nat. Commun. **10**, 1775 (2019).

[7] V. M. Edelstein, Phys. Rev. Lett. **75**, 2004 (1995).

[8] V. M. Edelstein, J. Phys.: Condens. Matter **8**, 339 (1996).

[9] S. Kanasugi and Y. Yanase, Phys. Rev. B **98**, 024521 (2018).

[10] D. Puggioni, G. Giovannetti, M. Capone, and J. M. Rondinelli, Phys. Rev. Lett. **115**, 087202 (2015).

[11] V. M. Edelstein, Phys. Rev. B **83**, 113109 (2011).

[12] V. P. Mineev and Y. Yoshioka, Phys. Rev. B **81**, 094525 (2010).

[13] V. M. Edelstein, Phys. Rev. B **72**, 172501 (2005).

[14] N. J. Laurita, A. Ron, J. Y. Shan, D. Puggioni, N. Z. Koocher, K. Yamaura, Y. Shi, J. M. Rondinelli, and D. Hsieh, Nat. Commun. **10**, 3217 (2019).

[15] H. Padmanabhan, Y. Park, D. Puggioni, Y. Yuan, Y. Cao, L. Gasparov, Y. Shi, J. Chakhalian, J. M. Rondinelli, and V. Gopalan, Appl. Phys. Lett. **113**, 122906 (2018).

[16] I. Sodemann and L. Fu, Phys. Rev. Lett. **115**, 216806 (2015).

[17] T. Low, Y. Jiang, and F. Guinea, Phys. Rev. B **92**, 235447 (2015).

[18] Q. Ma, S. Y. Xu, H. Shen, D. MacNeill, V. Fatemi, T. R. Chang, A. M. Mier Valdivia, S. Wu, Z. Du, C. H. Hsu, S. Fang, Q. D. Gibson, K. Watanabe, T. Taniguchi, R. J. Cava, E. Kaxiras, H. Z. Lu, H. Lin, L. Fu, N. Gedik, and P. Jarillo-Herrero, Nature **565**, 337 (2019).

[19] K. Kang, T. Li, E. Sohn, J. Shan, and K. F. Mak, Nat. Mater. **18**, 324 (2019).

[20] J. Son, K.-H. Kim, Y. H. Ahn, H.-W. Lee, and J. Lee, Phys. Rev. Lett. **123**, 036806 (2019).

[21] H. Wang and X. Qian, npj Comput. Mater. **5**, 119 (2019).

[22] J. Xiao, Y. Wang, H. Wang, C. D. Pemmaraju, S. Wang, P. Muscher, E. J. Sie, C. M. Nyby, T. P. Devereaux, X. Qian, X. Zhang, and A. M. Lindenberg, Nat. Phys. (2020), doi:10.1038/s41567-020-0947-0.

[23] H. Wang and X. Qian, Sci. Adv. **5**, eaav9743 (2019).

[24] J. Kim, K. W. Kim, D. Shin, S. H. Lee, J. Sinova, N. Park, and H. Jin, Nat. Commun. **10**, 3965 (2019).

[25] H. Sim and B. G. Kim, Phys. Rev. B **89**, 201107(R) (2014).

[26] H. J. Xiang, Phys. Rev. B **90**, 094108 (2014).

[27] H. M. Liu, Y. P. Du, Y. L. Xie, J. M. Liu, C.-G. Duan, and X. Wan, Phys. Rev. B **91**, 064104 (2015).

[28] J. Lu, G. Chen, W. Luo, J. Iniguez, L. Bellaiche, and H. Xiang, Phys. Rev. Lett. **122**, 227601 (2019).

[29] See Supplemental Material at http://link.aps.org/supplemental/10.1103/PhysRevB.102.024109 for detailed information on the Fermi surface and PDOS of ferroelectriclike LiOsO$_3$, symmetry analysis of Berry curvature dipole, Ohmic conductivity parameter C, and the relationship between Berry curvature dipole with Hubbard U, which includes Refs. [16,36,56–58].

[30] G. Kresse and J. Furthmüller, Phys. Rev. B **54**, 11169 (1996).

[31] G. Kresse and D. Joubert, Phys. Rev. B **59**, 1758 (1999).

[32] A. A. Mostofi, J. R. Yates, Y.-S. Lee, I. Souza, D. Vanderbilt, and N. Marzari, Comput. Phys. Commun. **178**, 685 (2008).

[33] A. A. Mostofi, J. R. Yates, G. Pizzi, Y.-S. Lee, I. Souza, D. Vanderbilt, and N. Marzari, Comput. Phys. Commun. **185**, 2309 (2014).

[34] Q. Wu, S. Zhang, H.-F. Song, M. Troyer, and A. A. Soluyanov, Comput. Phys. Commun. **224**, 405 (2018).

[35] J. R. Yates, X. Wang, D. Vanderbilt, and I. Souza, Phys. Rev. B **75**, 195121 (2007).

[36] W. C. Yu, X. Zhou, F.-C. Chuang, S. A. Yang, H. Lin, and A. Bansil, Phys. Rev. Mater. **2**, 051201(R) (2018).

[37] Y. Zhang, Y. Sun, and B. Yan, Phys. Rev. B **97**, 041101(R) (2018).

[38] J. I. Facio, D. Efremov, K. Koepernik, J. S. You, I. Sodemann, and J. van den Brink, Phys. Rev. Lett. **121**, 246403 (2018).

[39] D.-F. Shao, S.-H. Zhang, G. Gurung, W. Yang, and E. Y. Tsymbal, Phys. Rev. Lett. **124**, 067203 (2020).

[40] N. Nagaosa, J. Sinova, S. Onoda, A. H. MacDonald, and N. P. Ong, Rev. Mod. Phys. **82**, 1539 (2010).

[41] E. I. Paredes Aulestia, Y. W. Cheung, Y.-W. Fang, J. He, K. Yamaura, K. T. Lai, S. K. Goh, and H. Chen, Appl. Phys. Lett. **113**, 012902 (2018).

[42] A. Narayan, J. Phys.: Condens. Matter **32**, 125501 (2020).

[43] Y.-W. Fang and H. Chen, Commun. Mater. **1**, 1 (2020).

[44] S. Lei, M. Gu, D. Puggioni, G. Stone, J. Peng, J. Ge, Y. Wang, B. Wang, Y. Yuan, K. Wang, Z. Mao, J. M. Rondinelli, and V. Gopalan, Nano Lett. **18**, 3088 (2018).

[45] J. P. Castellan, B. D. Gaulin, J. van Duijn, M. J. Lewis, M. D. Lumsden, R. Jin, J. He, S. E. Nagler, and D. Mandrus, Phys. Rev. B **66**, 134528 (2002).

[46] I. A. Sergienko, V. Keppens, M. McGuire, R. Jin, J. He, S. H. Curnoe, B. C. Sales, P. Blaha, D. J. Singh, K. Schwarz, and D. Mandrus, Phys. Rev. Lett. **92**, 065501 (2004).

[47] P. Nukala, M. Ren, R. Agarwal, J. Berger, G. Liu, A. T. C. Johnson, and R. Agarwal, Nat. Commun. **8**, 15033 (2017).

[48] N. A. Benedek and T. Birol, J. Mater. Chem. C **4**, 4000 (2016).

[49] C. Ma and K. Jin, Sci. China: Phys., Mech. Astron. **61**, 97011 (2018).

[50] D. Puggioni and J. M. Rondinelli, Nat. Commun. **5**, 3432 (2014).

[51] Z. Z. Du, C. M. Wang, S. Li, H. Z. Lu, and X. C. Xie, Nat. Commun. **10**, 3047 (2019).

[52] E. J. König, M. Dzero, A. Levchenko, and D. A. Pesin, Phys. Rev. B **99**, 155404 (2019).

[53] S. Nandy and I. Sodemann, Phys. Rev. B **100**, 195117 (2019).

[54] C. Xiao, Z. Z. Du, and Q. Niu, Phys. Rev. B **100**, 165422 (2019).

[55] C. Xiao, H. Zhou, and Q. Niu, Phys. Rev. B **100**, 161403(R) (2019).

[56] S. S. Tsirkin, P. A. Puente, and I. Souza, Phys. Rev. B **97**, 035158 (2018).

[57] P. Liu, J. He, B. Kim, S. Khmelevskyi, A. Toschi, G. Kresse, and C. Franchini, Phys. Rev. Mater. **4**, 045001 (2020).

[58] Y. Zhang, J. Gong, C. Li, L. Lin, Z. Yan, S. Dong, and J.-M. Liu, Phys. Status Solidi RRL **12**, 1800396 (2018).